

Microstructural evolution in copper processed by severe plastic deformation

A. Mishra^a, V. Richard^b, F. Grégori^b, R.J. Asaro^a, M.A. Meyers^{a,*}

^a Department of Mechanical and Aerospace Engineering, University of California-San Diego, 9500 Gilman Drive, La Jolla, CA 92093-0411, USA

^b Laboratoire des Propriétés Mécaniques et Thermodynamiques des Matériaux - CNRS, Université Paris 13, 99, Av. J.-B. Clément, 93430 Villetaneuse, France

Received in revised form 8 April 2005

Abstract

The mechanisms of microstructural evolution in copper subjected to equal channel angular pressing (ECAP) have been investigated after successive passes. The first few passes are the most efficient in grain refinement while the microstructure becomes gradually more equiaxed as the number of passes increases. The texture evolution is discussed based on electron back scattered diffraction (EBSD) results. These experimental results are interpreted in terms of a preliminary model with four successive stages: homogeneous dislocation distribution; elongated sub-cell formation; elongated subgrain formation; break-up of subgrains into equiaxed units; sharpening of grain boundaries and final equiaxed ultrafine structure.

© 2005 Elsevier B.V. All rights reserved.

Keywords: Ultrafine grain; Misorientation angle; Thermomechanical history; Subgrain

1. Introduction

Prof. Langdon has been at the forefront of research in the field of creep and superplasticity for many years (e.g. [1–3]). More recently, he has concentrated his attention on severe plastic deformation techniques for creating ultrafine grain sized materials [4–6]. One widely accepted variant of severe plastic deformation is equal channel angular pressing (ECAP), that has been widely claimed as an effective process for producing ultrafine grain size (<1 μm) metals and alloys [7–10]. As the name suggests, ECAP involves use of a die that contains two intersecting channels of equal cross-section. The amount of strain that the sample experiences are dependent on two parameters: the inner angle of intersection of the channels, Φ , and outer angle of curve, Ψ [11]. Among the incentives for using this technique, the most important one is that the sample cross-section remains unchanged during processing. The final microstructure after processing is strongly dependent on the rotation scheme after consecutive passes [12–14]. The most widely used rotation schemes are, route A, where the billet is not

rotated between consecutive passes, route B_A, where the billet is rotated by 90° in alternate directions between consecutive passes, route B_C, where the billet is rotated by 90° in the same direction between consecutive passes and route C, where the billet is rotated by 180° between consecutive passes [15]. Studies on samples produced by these rotation schemes have shown that route B_C is the most effective route for producing equiaxed

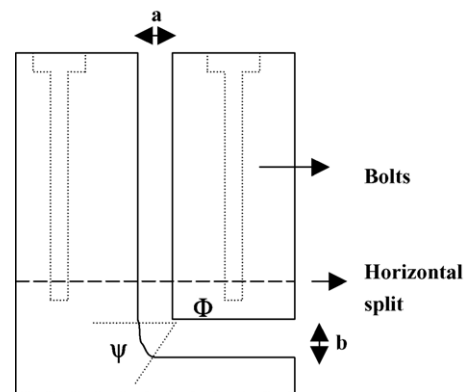


Fig. 1. Cross-section of die. Note that a and b are slightly larger than the channel diameter. Φ is the inner die angle and Ψ is the angle of the curved portion of the die.

* Corresponding author. Tel.: +1 858 534 4719; fax: +1 858 534 5698.
E-mail address: mameyers@mae.ucsd.edu (M.A. Meyers).

Table 1
Deformation paths and sequences

Die angle (°)	Number of passes								
	Route B _C						Route A	Route C	
90	1	2	3	4	6	8	10	8	8
102	1	2	3	4	6	8	–	8	8

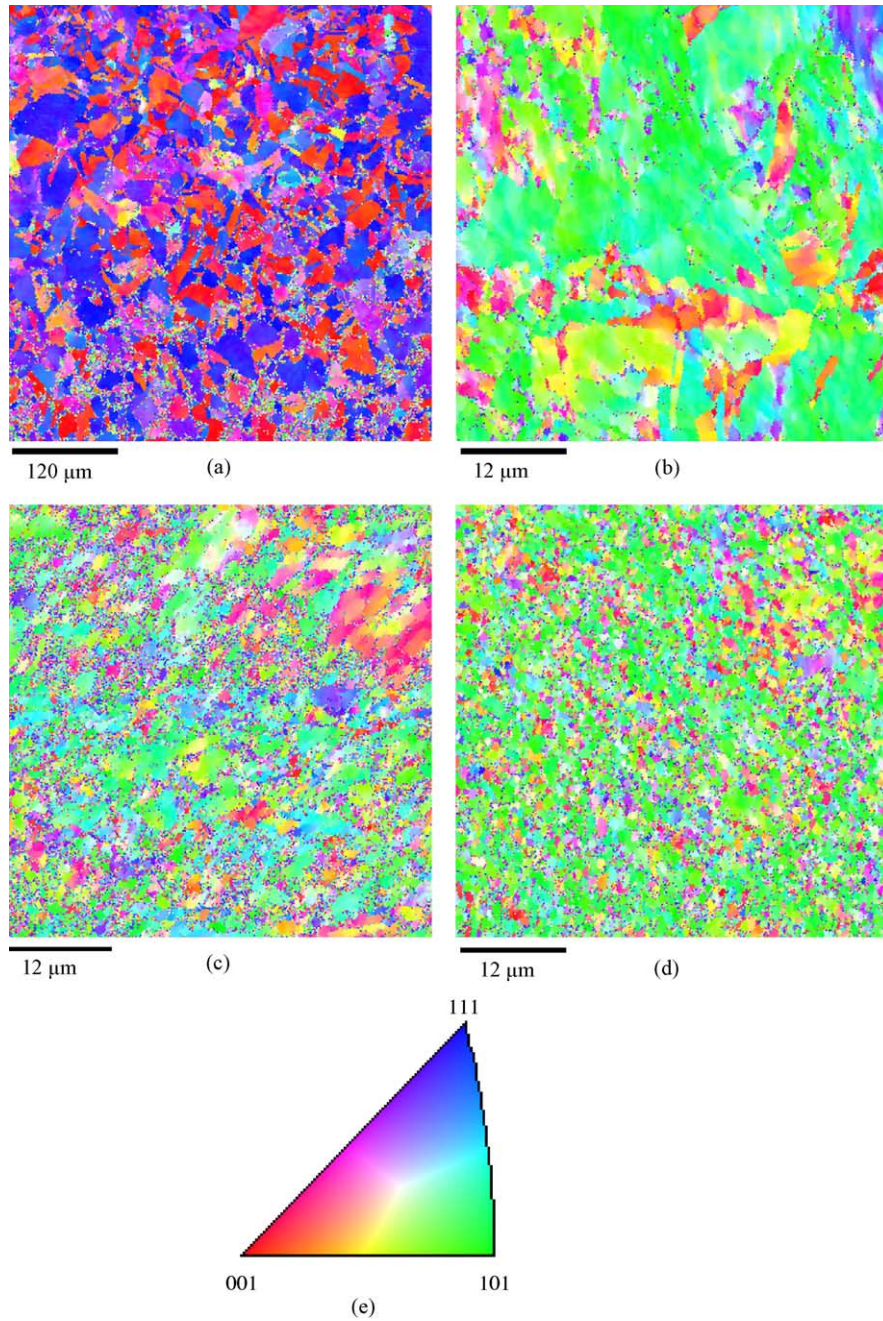


Fig. 2. Orientation maps for the samples produced from 102° die. (a) Initial condition, (b) two passes, (c) four passes, (d) eight passes and (e) representation of the color code used to identify the crystallographic orientations on standard stereographic projection (red: [001]; blue: [1 1 1]; green: [1 0 1]). Note the difference in scale for the initial condition; sample surface parallel to the extrusion axis. (For interpretation of the references to color in this figure legend, the reader is referred to the web version of the article.)

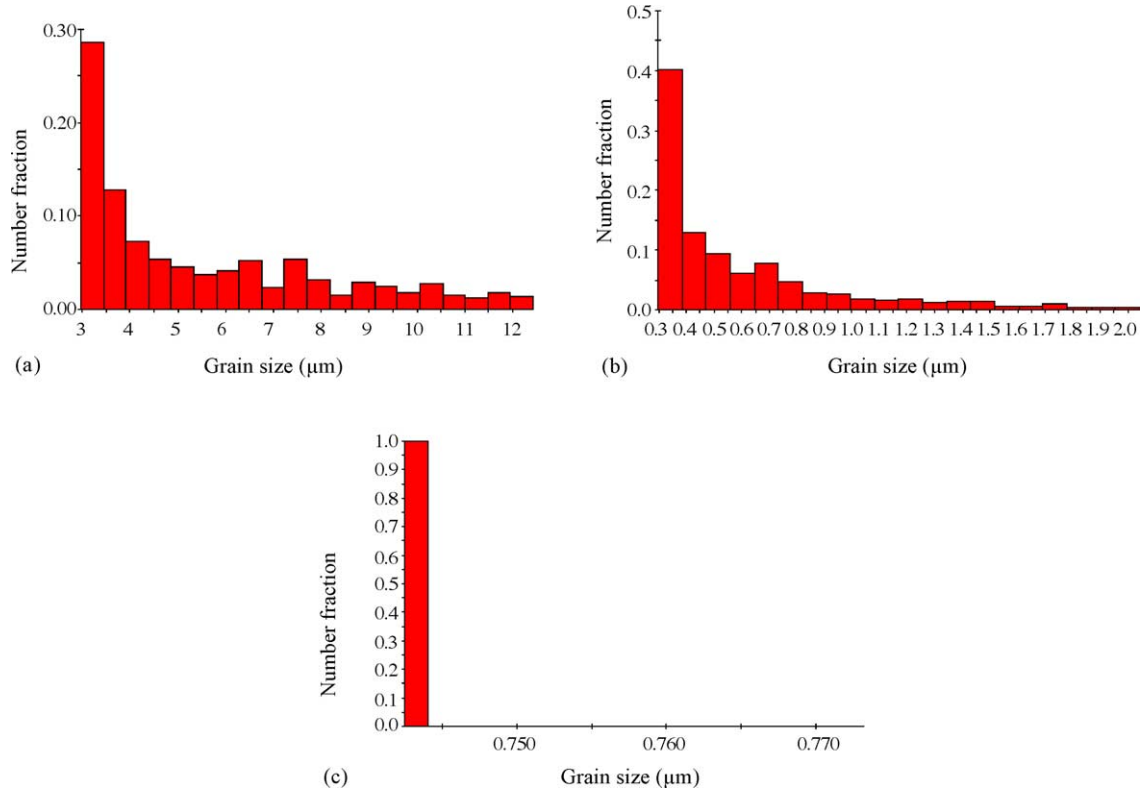


Fig. 3. Grain size distributions (from EBSD) for (a) initial condition, (b) two passes and (c) eight passes (samples produced from 102° die).

microstructure [16–19]. However, it should be mentioned that conflicting results have been reported (e.g. [20]).

The smaller the angle of intersection of the channels, Φ , the higher the strain induced in the sample leading to faster microstructural changes. The issue of the effectiveness of

different rotation schemes on the final microstructure remains unresolved. Several theories have been proposed to explain the mechanism of microstructural evolution during the shearing process. The goal of this paper is to present electron back scattered diffraction (EBSD) and transmission electron microscopy

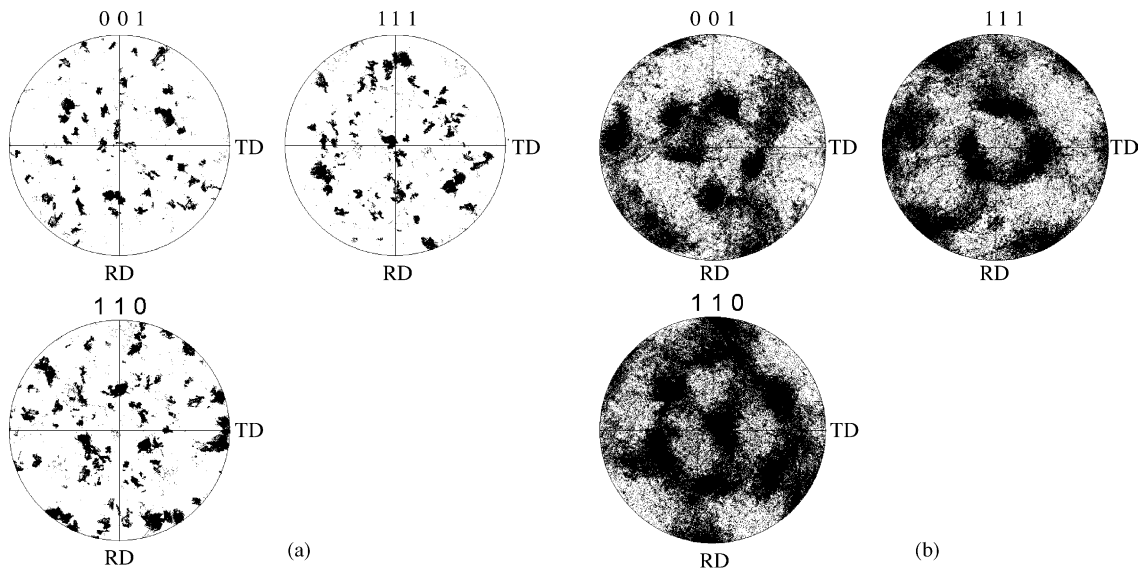
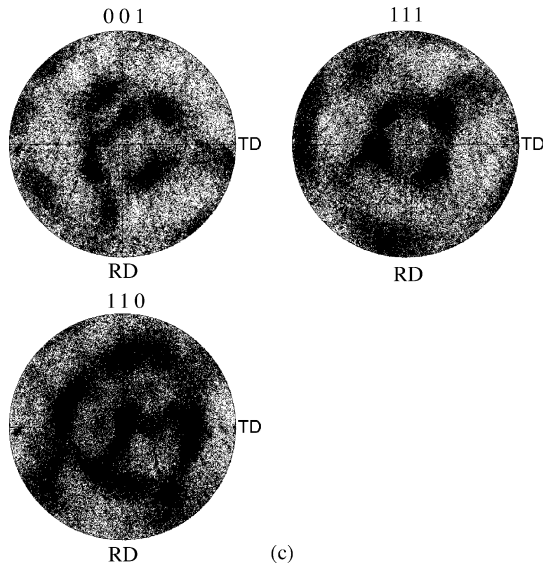


Fig. 4. Pole figures for (a) initial condition, (b) two passes and (c) eight passes (samples produced from 102° die).



(c)
Fig. 4. (Continued)

(TEM) results. Analysis of observations will be the topic of subsequent paper.

2. Experimental methods

ECAP dies with two different values of Φ (the inner angle of channel intersection) 90° and 102° were made. In most of the work reported, the dies are either single piece or have a vertical split. We used a unique design where the split was horizontal enabling replacement of the lower block with channels of different angles while the top piece is still reusable. A schematic of our die design is shown in Fig. 1 In both dies, the outer arc of curvature was a smooth 20° . With the exception of the entry and exit points, the channel diameter was uniformly 0.95 cm. The diameter was broadened at the entry and exit points to reduce friction. The initial samples of commercially pure Cu (purity $<99.9\%$) were cut into billets of 6.5 cm length and diameter that permitted loose fit in the channel. Pressing was carried out using H-13 tool steel plunger guided by a hydraulic press. The tolerance of the plunger was kept extremely low to prevent material from flowing in between the walls of the channel and the plunger.

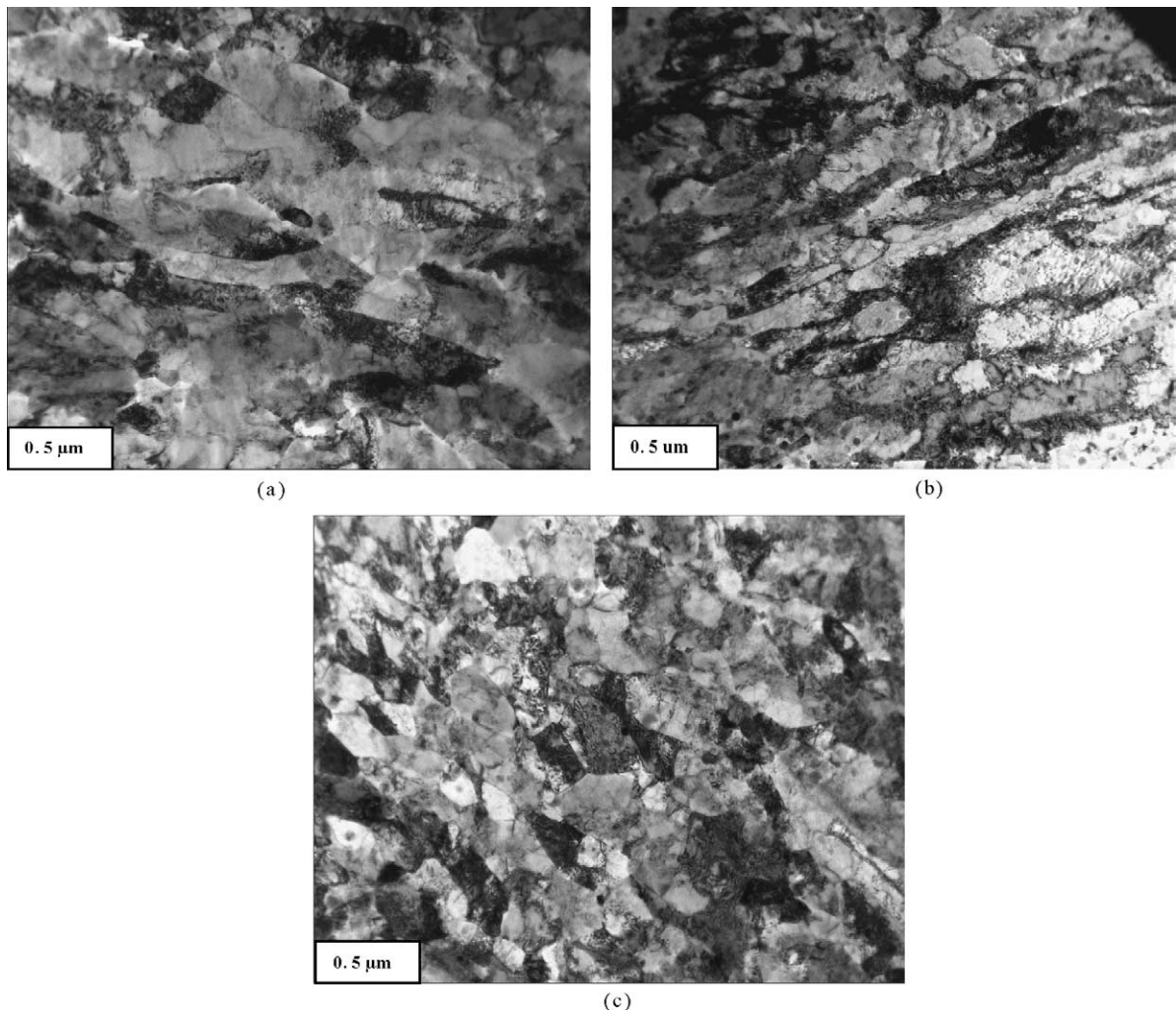


Fig. 5. Bright field TEM images (sample parallel to y axis) of samples produced from 90° die using three routes (eight passes); (a) route A no rotation, (b) route C 180° rotation and (c) route Bc 90° rotation.

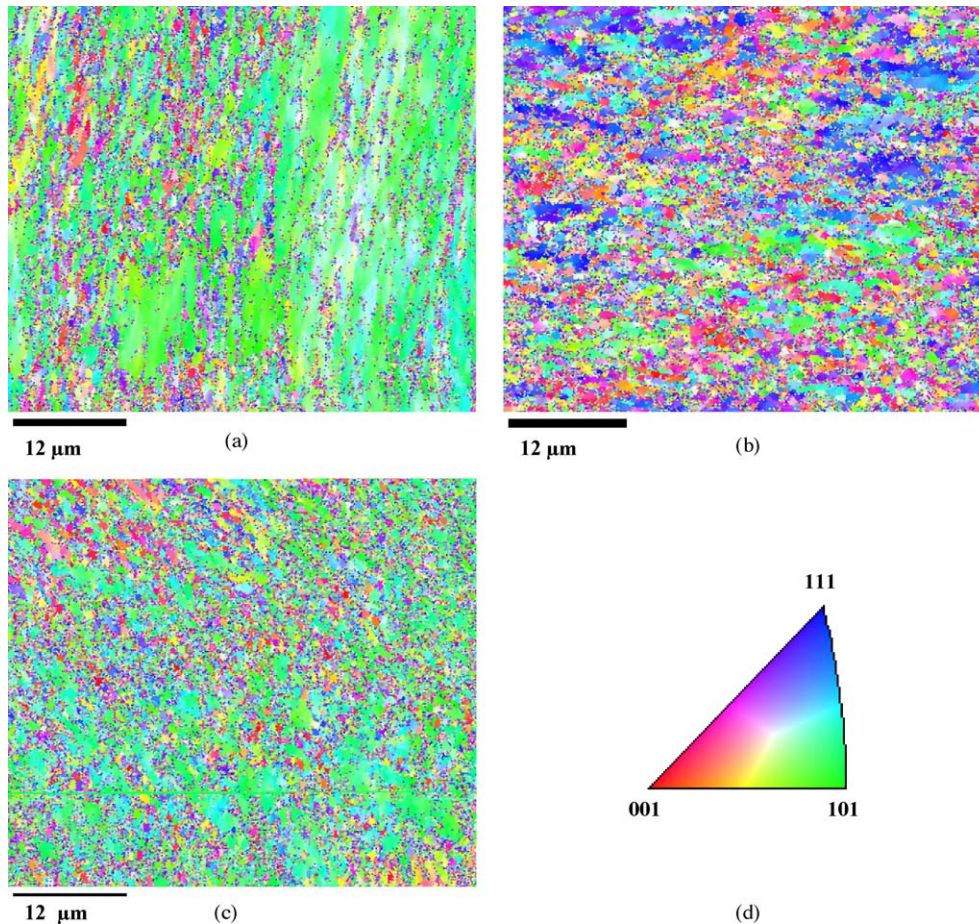


Fig. 6. Orientation maps for the samples produced from 90° die using three routes (eight passes): (a) route A no rotation, (b) route C 180° rotation, (c) route B_C 90° rotation and (d) representation of the color code used to identify the crystallographic orientations on standard stereographic projection (red: [0 0 1]; blue: [1 1 1]; green: [1 0 1]). (For interpretation of the references to color in this figure legend, the reader is referred to the web version of the article.)

Since several samples fitted in the channel at the same time, each Cu sample was alternated with an Al sample to reduce friction along the channel walls. Successive Cu samples would require a much higher load than intercalated Cu and Al samples. For the 102° die, load ~ 12 tonnes was required for the first two passes while subsequent passes needed ~ 10 tonnes. For the 90° die, the first two passes required ~ 20 tonnes while for subsequent passes the load dropped to ~ 15 tonnes. The billets and plunger were well lubricated before pressing. All modifications were primarily aimed at reducing friction since that is the main deterrent and leads to die and plunger failure as in our initial efforts. Table 1 outlines the choice of die angle, processing route and number of passes for the samples used in our work.

TEM analysis was carried out on 200 kV JEOL (JEM-2010, LaB₆). Observations were made on both transverse (y) and longitudinal (x or z no distinction was made between the two) directions. Crystallographic orientation analysis (using EBSD experiments) was done with TSL set up on Stereoscan 360 (Cambridge Instruments). The scanning parameters were set such that a grain boundary was defined when the misorientation between adjacent measurement points was higher than 15° . As a result, grain size, as predicted by EBSD data is shown to be smaller than

the actual value. To ensure precision, these results were used in combination with TEM to determine the correct value. For samples subjected to two or more passes, the measurement step size was reduced from 0.5 to $0.2 \mu\text{m}$ to capture the microstructural features. This led to a reduction of the scanning area to $50 \mu\text{m} \times 50 \mu\text{m}$ to complete the experiment in reasonable time.

3. Results and discussion

The initial grain size, measured by the linear intercept method (including annealing twin boundaries) was $17 \mu\text{m}$. The initial texture¹ ranged from (1 0 0) to (1 1 1) with the bigger grains having either (1 0 0) or (1 1 1) orientation. This can be clearly seen as blue and red grains in the inverse pole figure (IPF) (Fig. 2a). It is important to note that a large fraction of the grains refined to ultrafine size in the first two passes (60% grains $< 0.5 \mu\text{m}$, Fig. 3a and b). The texture starts evolving to (1 0 1) after two passes (indicated by green color in the IPF, Fig. 2b and d).

¹ Texture here does not refer to real texture but orientation of grain normal in the y direction.

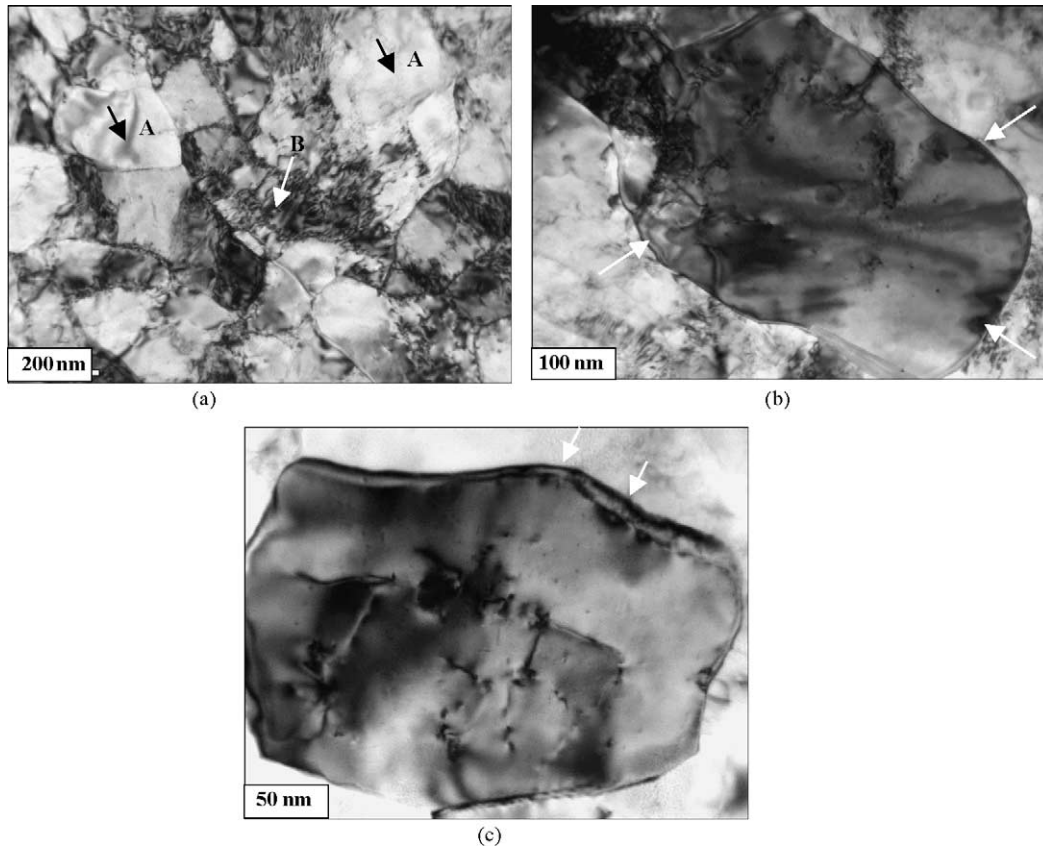


Fig. 7. Bright field TEM micrographs of sample after eight passes (route B_C): (a) showing inhomogeneous deformation, (b) and (c) dislocation activity within a grain.

This is clearly seen in the pole figure given in Fig. 4. Further passes lead to a reinforcement of the texture after two passes and progressively to a more equiaxed distribution of grains, after higher passes. Additionally, all the grains in the micrometer range are broken down to ultrafine size in higher number of passes. After eight passes, almost 100% structure is ultrafine (Fig. 3d).

The evolution of microstructure, especially texture from the initial condition to eight passes was found to be similar for samples produced from 90 and 102° dies. For 90° die, focus here is only on comparison between eight pass samples produced by different rotation schemes: routes B_C , A and C. As Fig. 5 shows, routes A and C produced elongated grains while route B_C resulted in a more equiaxed microstructure. The texture evolved to (1 0 1) in both route B_C and route A while it resulted mainly in (1 1 1) for route C (Fig. 6).

The samples processed by eight passes exhibited microstructural inhomogeneities, differences were observed in the features of grains lying in close vicinity. Additionally, inhomogeneity of deformation was also widely observed within individual grains. An area of a particular grain was found completely dislocation-free (arrows A, Fig. 7a) as opposed to a neighboring region that was heavily deformed (arrows B, Fig. 7a). This inhomogeneity in deformation could be related to misorientation within a grain. The grains with heavy dislocation

density break down to finer grains while the ones that are relatively low on dislocation density remain less affected. This could be the reason that the final ECAP processed microstructure shows an inhomogeneous distribution of grain sizes. The results obtained herein are in agreement with the ones reported by Iwahashi et al. [12,14] for aluminum. Another marked feature of the microstructure is the presence of non-equilibrium grain boundary configurations. Many grain boundaries were curved. This could be indicative of a mobility of the boundaries [e.g. 21,22]. This is shown by arrows in Fig. 7b and c.

4. Evolution of microstructure

The similarity between the microstructures produced by ECAP and the ones generated within adiabatic shear bands is striking, in spite of the significant differences in thermomechanical history. For comparison purposes, Fig. 8b shows the ultrafine grain sizes obtained in a hat-shaped specimen which constrained the plastic deformation in a narrow region with thickness of approximately 200 μm by Andrade et al. [23,24]. The shear strain imparted dynamically was approximately equal to 4. A grain size of $\sim 0.1 \mu\text{m}$ was produced. Fig. 8a shows the ECAP structure with equivalent shear strain (four passes). The grain size is fairly similar with a greater grain-boundary

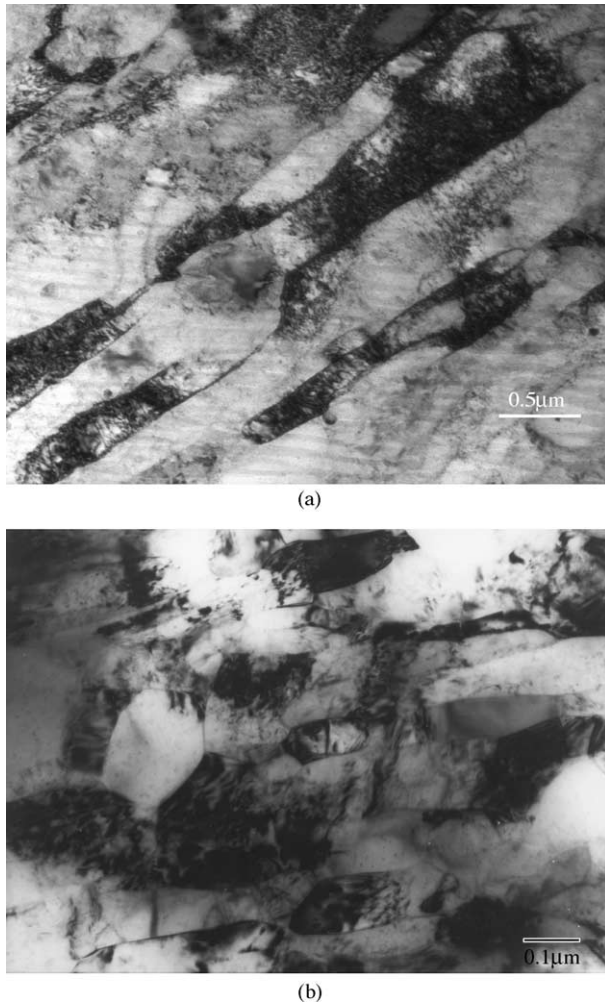


Fig. 8. TEM micrographs of Cu subjected to shear strain of four: (a) ECAP: two passes ($\sim \dot{\gamma} \approx 1 \text{ s}^{-1}$) and (b) hat-shaped specimen ($\dot{\gamma} \approx 10^4 \text{ s}^{-1}$).

waviness observed after ECAP. This is indeed surprising, considering the major differences in strain rate (approximately 1 s^{-1} for ECAP and 10^4 s^{-1} for hat-shaped specimen) and thermal history (successive thermal spikes after each pass for ECAP and adiabatic heating to $T = 600 \text{ K}$ for hat-shaped specimen).

A model for grain size refinement was proposed by Meyers et al. [25,26] for adiabatic shear bands. The principal features of this model are shown in Fig. 9. The sequence of events leading to the formation of the ultrafine grain size is self evident from Fig. 9a–e. A homogeneous dislocation distribution is replaced by energetically favorable subgrains. These subgrain walls present a barrier for dislocation propagation and the misorientation between adjacent grains increases gradually with plastic strain (Fig. 9c). Meyers et al. [25] showed that elongated subgrains are preferred over equiaxed ones and calculated the optimum aspect ratio. The thickness of these oblate spheroids ultimately determines the grain size; upon subdivision, the equiaxed structure is formed. Thermal energy assists in creating “clean” boundaries. One of the differences between Fig. 8a and b is that the grain

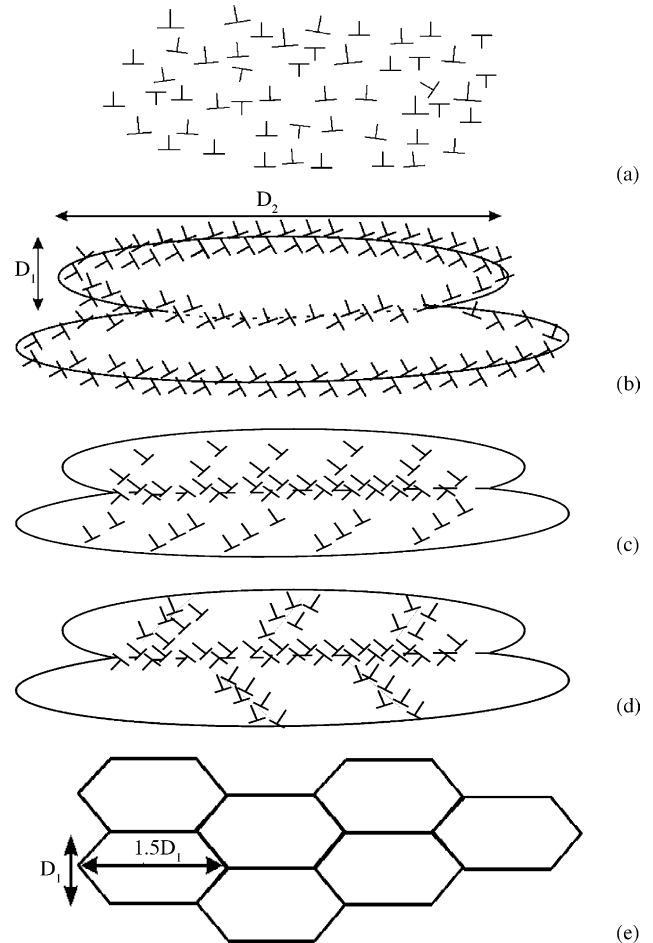


Fig. 9. Schematic illustration of microstructural evolution during severe plastic deformation. (a) Homogeneous distribution of dislocations, (b) elongated cell formation, (c) dislocations blocked by subgrain boundaries, (d) break up of elongated subgrains and (e) reorientation of subgrain boundaries and formation of ultrafine grain size.

boundaries are more curved (indicating mobility) in the ECAP produced sample. It is to be noted that the deformation time for shear band formation is extremely low ($\sim 2.5 \times 10^{-5} \text{ s}$) and temperature as high as 600 K is reached in the deformation process. On the other hand, during ECAP deformation time is high (to the order of a few seconds) while the expected temperature rise is much lower as compared to the shear band temperature rise. A detailed analysis is being carried out.

The path dependence of microstructural evolution, that has been firmly established in ECAP, has been analyzed by Zhu and Lowe [27]. The experiments carried out herein confirm that route B_C provides a more equiaxed grain structure than route A. A possible explanation for this is provided in Fig. 10. Repeated deformation along the same path (route A) should enhance the formation of elongated grains by increasing the misorientation angle between adjacent cells, then subgrains, then grains. On the other hand, if deformation is imparted by route B, after an initial pass, the shear strain will “break” the existing cells/subgrains, leading to a more rapid formation of the equiaxed structure.

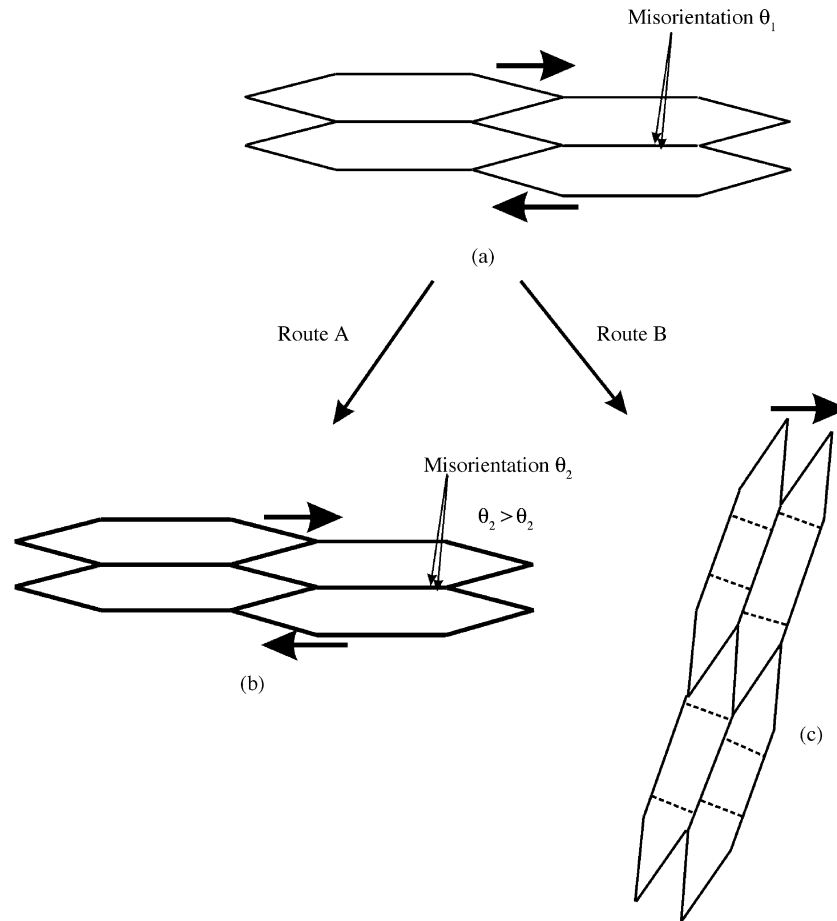


Fig. 10. Schematic showing the path dependence of microstructural evolution. (a) First pass, (b) subsequent pass in route A and (c) subsequent pass in route B.

5. Conclusions

ECAP is an effective process of producing ultrafine microstructure. The bulk of grain refinement seems to take place in the first few passes (two passes). This could be among the key steps in understanding the mechanism of grain refinement. In present work, the results obtained from 102 to 90° dies did not show any significant difference in the evolution of the microstructure as a function of number of passes. Change in texture is strong in the first few passes and it evolves in higher passes. The texture, which ranged from (1 0 0) to (1 1 1) in the initial condition of the sample, tends to (1 0 1) after ECAP using route B_C and route A while it tends to (1 1 1) using route C. Route B_C is more effective than both routes A and C for producing equiaxed microstructure. We observed inhomogeneity in deformation from one grain to the other and even within a grain. From our understanding this inhomogeneity in deformation could lead to an unequal distribution of grain size in the final microstructure.

A preliminary model for microstructural evolution leading to ultrafine grain formation is discussed. This model essentially establishes the size of the final ultrafine grain size as the minor axis of the oblate spheroids, which comprise the elongated cells.

Acknowledgments

Prof. Langdon was instrumental in giving us essential information leading to successful ECAP experiments. F. Grignon is gratefully acknowledged for his immense help during the ECAP set up process. This research is supported by the National Science Foundation under Grant CMS-0210173 (NIRT).

References

- [1] T.G. Langdon, *Acta Metall. Mater.* 42 (1994) 2437–2443.
- [2] T.G. Langdon, F.A. Mohamed, *Scripta Metall.* 10 (1976) 759–762.
- [3] T.G. Langdon, *Mater. Sci. Eng.* A174 (1994) 225–230.
- [4] M. Furukawa, Z. Horita, M. Nemoto, T.G. Langdon, *Mater. Sci. Eng.* A324 (2002) 82–89.
- [5] C. Xu, M. Furukawa, Z. Horita, T.G. Langdon, *J. Alloys Compd.* 22 (2004) 27–34.
- [6] Z. Horita, T. Fujinami, T.G. Langdon, *Mater. Sci. Eng.* A318 (2001) 34–41.
- [7] R.Z. Valiev, N.A. Krasilnikov, N.K. Tsenev, *Mater. Sci. Eng.* A137 (1991) 35.
- [8] R.Z. Valiev, E.V. Kozlov, Y.U.F. Ivanov, J. Lian, A.A. Nazarov, B. Budalet, *Acta Metall. Mater.* 42 (1994) 2467.
- [9] J. Wang, M. Furukawa, Z. Horita, M. Nemoto, R.Z. Valiev, T.G. Langdon, *Mater. Sci. Eng.* A216 (1996) 41.

- [10] J. Wang, Y. Iwahashi, Z. Horita, M. Furukawa, M. Nemoto, R.Z. Valiev, T.G. Langdon, *Acta Mater.* 44 (1996) 2973.
- [11] M. Furukawa, Y. Ma, Z. Horita, M. Nemoto, R.Z. Valiev, T.G. Langdon, *Mater. Sci. Eng. A241* (1998) 122.
- [12] Y. Iwahashi, Z. Horita, M. Nemoto, T.G. Langdon, *Acta Mater.* 45 (1997) 4733.
- [13] S. Ferrasse, V.M. Segal, K.T. Hartwig, R.E. Goforth, *Metall. Mater. Trans. A28* (1997) 1047.
- [14] Y. Iwahashi, Z. Horita, M. Nemoto, T.G. Langdon, *Acta Mater.* 46 (1998) 3317.
- [15] M. Furukawa, Y. Iwahashi, Z. Horita, M. Nemoto, T.G. Langdon, *Mater. Sci. Eng. A257* (1998) 328.
- [16] T.G. Langdon, M. Furukawa, M. Nemoto, Z. Horita, *J. Organomet. Chem.* 52 (2000) 30.
- [17] Y. Iwahashi, Z. Horita, M. Nemoto, T.G. Langdon, *Acta Mater.* 46 (1998) 3317.
- [18] K. Oh-Ishi, Z. Horita, M. Furukawa, M. Nemoto, T.G. Langdon, *Metall. Mater. Trans. A29* (1998) 2011.
- [19] Y. Iwahashi, Z. Horita, M. Nemoto, T.G. Langdon, *Acta Mater.* 45 (1997) 4733.
- [20] P.B. Pragnell, A. Gholinia, V.M. Markushev, in: T.C. Lowe, R.Z. Valiev (Eds.), *Investigations and Applications of Severe Plastic Deformation*, Kluwer Academic Publications, Dordrecht, 2000, pp. 65–71.
- [21] J. Gil Sevillano, P. van Houtte, E. Aernoudt, *Prog. Mater. Sci.* 25 (1981) 69–412.
- [22] F. J. Humphreys, M. Hatherly, *Recrystallization and Related Phenomena*, Oxford, UK, 1995.
- [23] U.R. Andrade, M.A. Meyers, K.S. Vecchio, A.H. Chokshi, *Acta Metall. Mater.* 42 (1994) 3183.
- [24] M.A. Meyers, U. Andrade, A.H. Chokshi, *Metall. Mater. Trans. A26* (1995) 2881.
- [25] M.A. Meyers, J.C. LaSalvia, V.F. Nesterenko, Y.J. Chen, B.K. Kad, in: T.R. McNelley (Ed.), *Recrystallization and Related Phenomena, Rex'96*, Montery, 1997, pp. 279.
- [26] M.A. Meyers, V.F. Nesterenko, J.C. LaSalvia, Q. Xue, *Mater. Sci. Eng. A317* (2001) 204–225.
- [27] Y.T. Zhu, T.C. Lowe, *Mater. Sci. Eng. A291* (2000) 46–53.